Remote Sens. **2010**, *2*, 1400-1415; doi:10.3390/rs2051400

OPEN ACCESS

Remote Sensing

ISSN 2072-4292

www.mdpi.com/journal/remotesensing

Article

Satellite and Ground-Based Sensors for the Urban Heat Island Analysis in the City of Rome

Roberto Fabrizi [1], Stefania Bonafoni [1,*] and Riccardo Biondi [2]

[1] Department of Electronic and Information Engineering, University of Perugia, via G. Duranti 93, 06125 Perugia, Italy; E-Mail: roberto8031@hotmail.com

[2] DTU Space, National Space Institute, Juliane Maries Vej 30, 2100, København Ø, Denmark; E-Mail: ribi@space.dtu.dk

* Author to whom correspondence should be addressed; E-Mail: stefania.bonafoni@diei.unipg.it; Tel.: +390-755-853-663; Fax: +390-755-853-654.

Received: 21 February 2010; in revised form: 28 April 2010 / Accepted: 14 May 2010 / Published: 20 May 2010

Abstract: In this work, the trend of the Urban Heat Island (UHI) of Rome is analyzed by both ground-based weather stations and a satellite-based infrared sensor. First, we have developed a suitable algorithm employing satellite brightness temperatures for the estimation of the air temperature belonging to the layer of air closest to the surface. UHI spatial characteristics have been assessed using air temperatures measured by both weather stations and brightness temperature maps from the Advanced Along Track Scanning Radiometer (AATSR) on board ENVISAT polar-orbiting satellite. In total, 634 daytime and nighttime scenes taken between 2003 and 2006 have been processed. Analysis of the Canopy Layer Heat Island (CLHI) during summer months reveals a mean growth in magnitude of 3–4 K during nighttime and a negative or almost zero CLHI intensity during daytime, confirmed by the weather stations.

Keywords: Urban Heat Island; satellite remote sensing; weather stations; air temperature

1. Introduction

Since the early 1960s, numerous satellite sensors have been launched into orbit to observe and monitor the Earth and its environment. During the years, technologies have improved considerably and the number of satellite missions has increased. Among the several remote sensing applications, a

relatively new one is the study of urban areas, in which the surface temperature is of primary importance to the study of urban climatology.

Over the last century, the world has witnessed a huge growth in its population; almost all of the predicted world population growth over the next 30 years will be concentrated in urban areas. This intense and relatively fast-paced increase in urban population changes the characteristics of the Earth's surface and atmosphere.

Anthropogenic activities induce changes in the physical characteristics of the surface (albedo, thermal capacities, heat conductivity, moisture) and have significant implications for the local energy budget [1]. The removal of natural land cover and the introduction of artificial materials, such as concrete and asphalt, modify the surface energy balance, resulting in an increase in surface temperature; this creates an increase in sensible heat flux and a resultant rise in air temperature. Heat retention from artificial surfaces impacts the natural energy balance and can worsen existing air pollution conditions. Thus, as cities add more roads, buildings, industries and people, temperatures in downtown areas become much higher than temperatures in rural surroundings, creating the Urban Heat Island (UHI) phenomenon [2].

The UHI describes quantitatively the increased temperature of either the urban surface or the urban atmosphere compared to its rural surroundings. The temporal and spatial characteristics of the UHI vary with changes in local urban form and function. Local meteorological conditions, geography (topography, presence of water bodies such as lakes or rivers, soil types, *etc.*) also affect the magnitude of an UHI. Also, population, as a surrogate measure of the density of urban living, was originally linked to UHI intensity [3].

There are three types of UHI [2]:

- Canopy Layer Heat Island (CLHI);
- Boundary Layer Heat Island (BLHI);
- Surface Heat Island (SHI).

The CLHI and the BLHI refer to a warming of the urban atmosphere whereas the SHI refers to a warming of the surface. The urban canopy layer is the layer of air closest to the surface in cities, extending upwards to approximately the mean building height. Above the canopy layer lays the urban boundary layer, which may be 1 km or more in thickness at daytime, shrinking to hundreds of meters or less at night. These components are depicted in Figure 1.

The CLHI are typically detected by ground stations using thermometers in order to measure air temperature in the canopy layer whereas the thermal remote sensors observe the surface heat island or, more specifically, they see the spatial patterns of upwelling thermal radiance received by the detector and use it to estimate the surface temperature [4].

UHI's have long been studied by ground-based observations taken from fixed thermometer networks. An alternative method uses infrared radiometry from aircraft or satellite platforms. An advantage in using satellite data with respect to ground-based observations is to provide more spatially representative measurements of surface temperature over large areas of cities. The conceptual framework of employing satellite remote sensing data for surface UHI assessment was originally employed by Rao [5].

Figure 1. Schematic of the main components of the urban atmosphere.

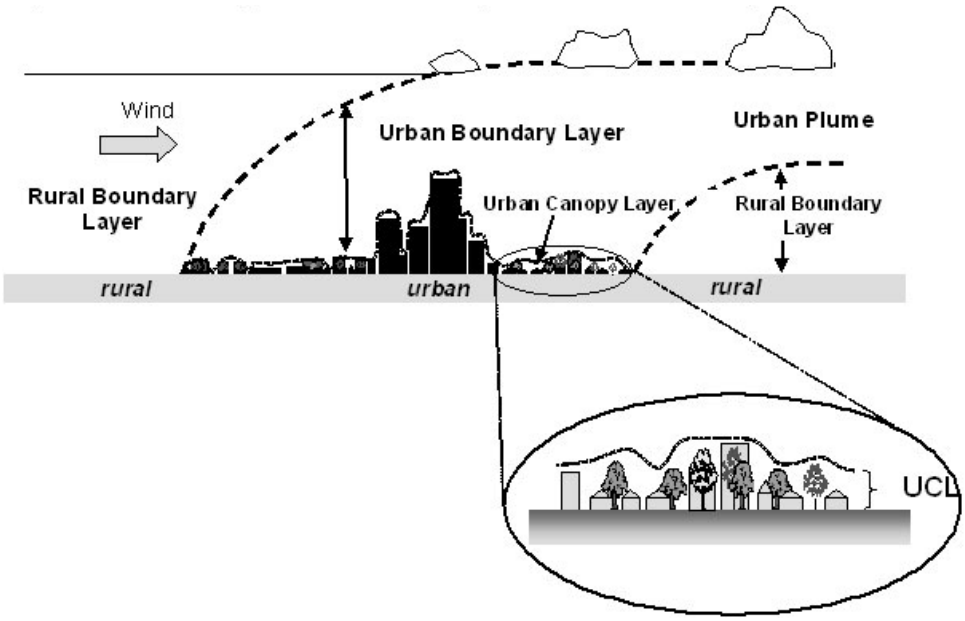

Inspired by his work, research was pursued to understand the energetic basis of this phenomenon through field observations and numerical and scale modeling of the energy exchanges of urban and rural environments [1]. To extend the database of work, UHI's were studied in several cities, such as Houston [6], Seoul [7], Los Angeles and Paris [8].

Streutker [6] studied the UHI by the use of nighttime NOAA (US National Oceanic and Atmospheric Administration)-AVHRR (Advanced Very High Resolution Radiometer) thermal data in order to produce surface temperature maps of the city of Houston for 21 selected dates covering a two year period (1998–1999). He found the surface UHI intensity ranging from 1.06 to 4.25 °C depending on season and weather conditions.

Lee [7] examined the potential of using the NOAA-AVHRR thermal data to map the pattern of brightness temperature distribution in order to study surface urban heat islands in the Seoul metropolitan area. He located the warm areas during daytime, associated with business activities and industrial and densely residential districts. Lee figured out that the AVHRR-derived brightness temperatures were highly correlated with the ground surface temperature and the surface air temperature, therefore he supported the potential of utilizing the AVHRR data to retrieve the air and ground surface temperature fields in a city to evaluate the urban heat island.

Dousset and Gourmelon [8] studied the summertime microclimate of the Los Angeles and Paris metropolitan areas by combining satellite multi-sensors data with *in situ* air quality in a Geographic Information System (GIS) platform. They used the NOAA-AVHRR thermal data corresponding to various times of day in order to produce images of average surface temperature from which statistics were extracted. In addition, they used SPOT (Satellite Pour l'Observation de la Terre)-HRV (High Resolution Visible) visible and near infrared measurements at a 20-m spatial resolution to estimate the land cover classification for the cities. The study revealed a strong UHI of 7 °C for Paris at night and a "negative" surface UHI during the day, where commercial/industrial and airport regions as well as densely suburbs displayed higher surface temperature than downtown Paris. For the city of Los Angeles, the statistics of the diurnal cycle of Land Surface Temperature (LST) as derived from the

average images highlighted a strong heat island in the range of 7.5–9 °C during the day and a weaker heat island in the range of 2–5 °C at night, which was attributed to the influence of the Pacific Ocean.

Hung *et al.* [9] utilized TERRA-MODIS (Moderate Resolution Imaging Spectroradiometer) image data to assess the UHI of eight mega-cities in Asia. They used both daytime and night-time MODIS data acquired over 2001–2003 period to produce surface temperature maps for the eight cities at 1 km spatial resolution. The diurnal and seasonal patterns of the satellite-derived UHIs revealed that all cities exhibited significant heat islands. The correlation between heat islands and surface properties as well as the relationship between UHI magnitude and city population was also determined.

In this paper, we study the spatial and temporal evolution of canopy layer UHI in the city of Rome, combining air temperature observations from the meteorological urban sensor network and both daytime and nighttime data from the satellite-based sensor AATSR (Advanced Along Track Scanning Radiometer) to produce temperature maps.

2. Study Area

The urban area of this study is Rome, Italy, a city of 3.7 million people. It is located in the central-western portion of the Italian Peninsula, in a valley enclosed by the Apennines Mountains: the Tolfa Mountains lie to the North, the Sabatini Mountains to the East and the Colli Albani to the South. Figure 2(a) shows the area investigated and locations of the weather stations employed in this study. The city of Rome covers an overall area of about 1,285 km^2, placed inside the motorway orbital road "Grande Raccordo Anulare" (orange ring). Its altitude ranges from 13 to 120 m above mean sea level.

Figure 1. (a) Study area of Rome with the employed weather stations across Rome. Urban weather stations are marked A-G, and rural station with a green star. (b) The periods of significant growth of Rome, starting from top: 1951, 1964, 1977, 1991.

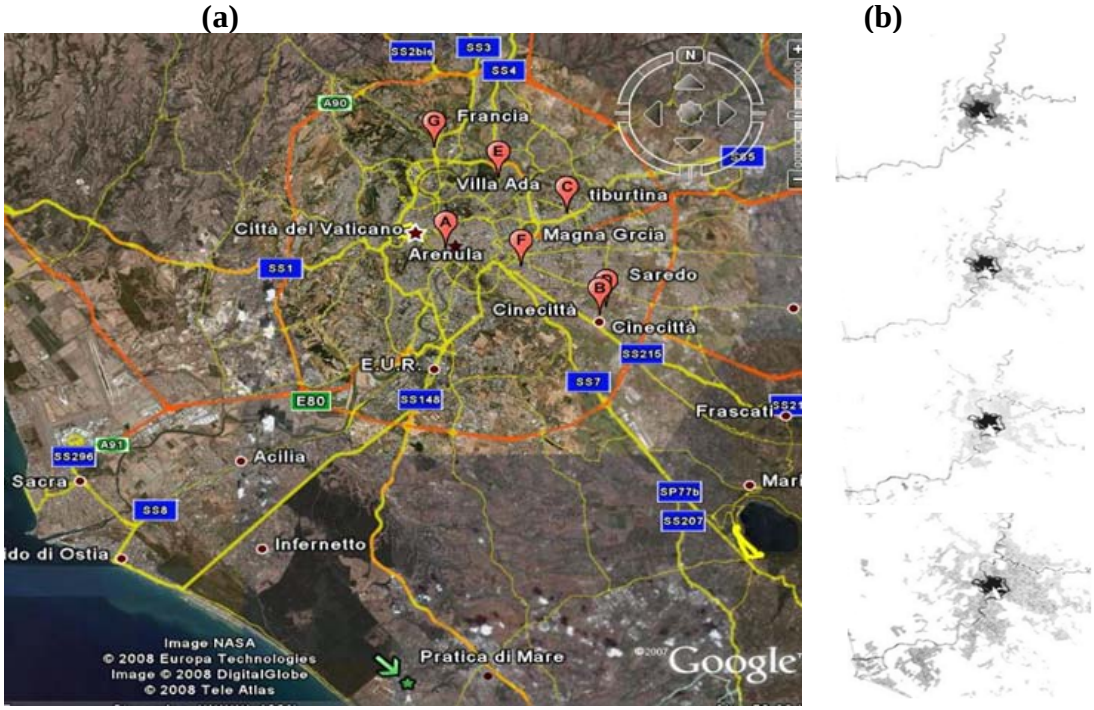

Rome enjoys a typical Mediterranean climate, which is characterized by relatively mild winters and hot summers. The climate is fairly comfortable from April through June, and from mid-September to October. In August, the temperature during the heat of the day often exceeds 32 °C; the average high temperature in December is about 14° C, while subzero lows are not uncommon [10].

In the years after the Second World War, Rome underwent the most significant urban growth of its history. The population grew from 1,500,000 to 2,800,000 in approximately 25 years, from 1945 to 1971, due to the huge flux of immigration. Between 1951 and 1971 this rise consequently raised the number of houses from 320,000 to 870,000, as sketched in Figure 2(b). During these years the city grew chaotically with little town planning, which resulted in deep modifications to the landscape within the built areas and the nearby suburbs. In fact, Rome is composed of a more elaborate urban lattice with buildings showing a variety in heights (from 4 to 12 storeys); this implies multiple surfaces for the reflection and absorption of sunlight increasing the efficiency at which urban areas can be heated. This is called the canyon effect. In addition, buildings tend to block the wind, inhibiting cooling by convection [4].

3. Sensor Description

3.1. Satellite-Based Sensors: AATSR and MERIS

In this work, we used observations provided by the Advanced Along-Track Scanning Radiometer (AATSR) and the MEdium Resolution Imaging Spectrometer (MERIS) [11], onboard the ENVISAT satellite. ENVISAT was launched in 2002, and is the biggest Earth remote sensing project of the European Space Agency (ESA). It flies in a sun-synchronous polar orbit at roughly 800-km altitude, and provides complete coverage of the globe every three days.

The Advanced Along-Track Scanning Radiometer was designed primarily to study the Sea Surface Temperature (SST) with high accuracy; but, it has been successfully used for land, atmosphere, cloud and cryosphere applications [12]. The AATSR is a multispectral radiometer providing data products with a resolution of 1 km at nadir derived from measurements at seven different wavelengths in visible and infrared channels (in the range 0.55 μm to 12 μm). A special technique is used to allow observations of each surface location from two different angles, at 55 degrees from vertical (the forward view) and at an angle close to the vertical (the nadir view). The swath width is constant at 500 km [11]. In this work, level 1b products ATS_TO_1P, comprising gridded brightness temperature and reflectance (GBTR) images, were acquired from ESA. These images provide calibrated and geolocated brightness temperatures from all three infrared channels, reflectances from the near-infrared and visible channels, and information on whether the surface is land or ocean [13].

MERIS is a passive, programmable, imaging spectrometer, which operates in the solar reflective spectral range. Fifteen spectral bands can be selected by ground command in the range 390 nm to 1,040 nm with variable bandwidth from 1.25 nm to 30 nm; therefore, observations are nominally limited to the day side of the Earth. The instrument scans the Earth's surface by the 'push broom' method (68.5 degrees field of view) with a 1,150-km swath width [11].

The main objective of MERIS is the study of ocean color and the role of the ocean in the climate system. In addition, is used for atmospheric monitoring to detect cloud properties, water vapor and aerosol for land use [14]. Two different product resolutions are available, full resolution (FR, about

300 m) and reduced resolution (RR, about 1 km). In this work we used MERIS level 2b RR geophysical products (MER_RR_2P) which provide cloud mask information at a resolution of 1.2 km [15].

Both sensors (AATSR and MERIS) offer a synergistic potential that contributes to climate studies and global change observations in addressing environmental features in a multi-disciplinary way. Since they are co-located in the same platform, they observe almost the same scene at the same time.

3.2. Ground-Based Sensors: Meteorological Weather Station

Ground-based meteorological weather stations, managed by the ARPA Lazio (Regional Agency for Environmental Protection), were used in order to measure air temperature in the Rome area (http://www.arpalazio.net/main/). The stations are placed at around 2 m above the ground, equipped with anemometer, thermometer, hygrometer, barometer, rain gauge, pyranometer; measurements from these sensors are collected every hour, archived and quality checked by ARPA Lazio. The thermometer (HMP 45C, Vaisala) measurement range is −35 °C to +60 °C with an accuracy of around ±0.2 °C. Details on station location and data availability are provided in the next section.

4. Sensor Data Selection

4.1. Data from AATSR and MERIS

MERIS level 2b and AATSR level 1b data were provided by ESA, selecting pixels inside of a circle with radius of 20 km centered in the center of Rome at coordinates 41°53′N 12°29′E. MERIS has been used for cloud detection identifiable by a flag parameter presence in the MERIS data (if cloud type is equal to zero the pixel is cloudless), whereas the AATSR sensor has been used in order to estimate the air temperature by brightness temperatures from AATSR 11 μm and 12 μm channels over Rome between 2003 and 2006, as reported in Table 1.

Only data from AATSR nadir view were considered in order to reduce the impact of the atmosphere on measurements. In fact, the observations made in forward view are more susceptible to atmospheric scattering and absorption than in the nadir view because the path length is approximately twice that of the nadir view [16].

Since both AATSR and MERIS share the same platform, the data are spatially and temporally co-registered. This allows products to be processed by combining the thermal channels of AATSR and the multi-spectral information of MERIS [17].

Table 1. ENVISAT satellite sensors: data set available.

Sensor	Level	Period
AATSR	Level 1b	2003–2006
MERIS	Level 2b	2002–2006

4.2. Data from Meteorological Weather Stations

Data from ground-based meteorological weather stations were collected in order to directly measure air temperature in the canopy layer using thermometers. Table 2 reports the eight stations employed in this study, provided from the ARPA Lazio, and the time period of data availability. The temporal

resolution of the temperature data is one hour. As displayed in the Figure 2(a), the urban ground stations are all situated around the center of Rome and are all built upon an asphalt surface, except for the Villa Ada station which is situated at the edge of a park (Villa Ada park). For the rural area, data was collected at Pratica di Mare station (the only one available as rural from ARPA Lazio). Anyway, this station can be considered an acceptable representative of the flat rural area surrounding Rome.

Table 2. Meteorological weather stations of ARPA Lazio and time period of data availability.

Station	Type	Period
Arenula	Urban	01/01/2001–01/11/2006
Francia	Urban	30/06/2004–01/11/2006
Tiburtina Vecchia	Urban	01/01/2003–27/10/2006
Villa Ada	Urban in a park	01/01/2001–01/11/2006
Cinecittá	Urban	01/01/2003–01/11/2006
Magna Grecia	Urban	01/01/2001–01/11/2006
Saredo	Urban	01/01/2003–31/12/2006
Pratica di Mare	Rural	01/01/2003–01/12/2006

5. Regression Analysis

5.1. Literature Formulation

Surface temperature and canopy layer temperature are important factors controlling most physical, chemical and biological processes on Earth. Knowledge of these geophysical parameters is necessary for many environmental studies and management of Earth surface resources.

Different approaches have been published in the last years in order to retrieve sea and land surface temperature (SST and LST) from satellite-derived radiances [18-22]. Among these methods, the two-channel or split-window algorithms have been the most commonly used [18,21,23]. The split-window technique refers to the different atmospheric attenuation suffered by the surface emitted radiance within the atmospheric window 10–12.5 μm [18].

This implies that the split-window algorithms take advantage of the differential absorption in two close infrared channels to correct for the atmospheric effects, describing the surface temperature in terms of a linear combination of brightness temperatures measured in both thermal channels. The following Equation (1) is the general formula for the split-window algorithms:

$$T_s = a_0 + \sum_{i=1}^{n} a_i T_i \tag{1}$$

where T_s is the LST and T_i are the brightness temperatures of two close thermal infrared channels; the coefficients depend on the atmospheric state and on the surface emissivity and they are chosen in order to minimize the error in the LST determination. Numerous studies have been done to estimate these coefficients over sea and land surface; but, sometimes fixed values are utilized, imposing significant errors to the results [24].

In this framework, an objective of the present paper is to find the most appropriate split-window algorithm from literature in order to study the UHI in Rome, or to propose a more suitable optimization of the split-window technique for the area under investigation.

Three different split-window formulations for LST found in the literature have been analyzed and compared with ground data. These are hereafter named Price [21], Ulivieri [23] and Prata & Platt [25]. Although these algorithms were originally implemented with data from the AVHRR on board the NOAA polar orbiting satellites, in this work they have been tested by using the brightness temperatures from the thermal infrared AATSR channels (hereafter T_{11} and T_{12}), *i.e.*, the channels 11 and 12 centered at 10.8 μm and 12 μm with a bandwidth of 1 μm. It is important to emphasize that the original AVHRR channels employed in the algorithm formulations, *i.e.*, channels 4 and 5, have the same central frequencies of the AATSR, with also the same bandwidths.

With reference to the algorithms reported in Table 3, we assumed the surface emissivity as $\varepsilon_{11} = 0.95$ and $\varepsilon_{12} = 0.96$, typical mean values for urban areas [26-29], where again the subscripts refer to channels 11 and 12 of AATSR.

The resultant land surface temperature has been compared with the air temperature from Cinecittà ground weather station by selecting the AATSR pixel covering the weather station location. The ENVISAT satellite passes over Rome around 9:00–10:00 and 20:00–21:00 UTC. To perform this comparison only cloud-free data were utilized, since the presence of clouds carries a decrease in the brightness temperature [27].

The results are presented in Table 3, employing AATSR brightness temperatures and weather station air temperatures for the period reported in Table 2 for the Cinecittà station. The three dissimilar root mean square (rms) differences between the estimated T_s and the measured air temperature at 2 m above the ground yields an uncertainty in the evaluation of the capability of these algorithms in the estimation of urban surface temperature, and therefore an uncertainty in their applicability for the Rome area.

Table 3. Split-window algorithms with T_s, T_{11}, T_{12} in K, $T_0 = 273.15$ K, $\varepsilon = (\varepsilon_{11} + \varepsilon_{12})/2$, $\Delta\varepsilon = (\varepsilon_{11} - \varepsilon_{12})$. The last column is the rms difference between the estimated T_s and the measured air temperature in Rome.

Authors	Algorithms	Rms difference (K)
Price [21]	$T_s = \left[T_{11} + 3.33(T_{11} - T_{12})\right] * \left[\frac{5.5 - \varepsilon_{11}}{4.5}\right] + 0.75 T_{12} \Delta\varepsilon$	18.20
Ulivieri [23]	$T_s = \left[T_{11} + 1.8(T_{11} - T_{12})\right] + 48(1 - \varepsilon) - 75\Delta\varepsilon$	13.85
Prata & Platt [25]	$T_s = 3.45\frac{T_{11} - T_0}{\varepsilon_{11}} - 2.45\frac{T_{12} - T_0}{\varepsilon_{12}} + 40\frac{(1 - \varepsilon_{11})}{\varepsilon_{11}} + T_0$	16.11

5.2. New Formulation

In order to employ a method for the evaluation of the UHI in Rome with less uncertainty, we have developed a local and more suitable algorithm for the estimation of the CLHI. This method exploits the availability of air temperature data from ground-based weather stations in the study's area.

In general, there are two approaches solving the problem of determining surface temperature using the split-window channels. The first assumes that the effects due to land and atmosphere can be decoupled and then the method is to separate out the surface effects (emissivity) from the atmospheric effects (water vapor). The second approach is to accept that the surface and atmosphere are coupled

and then the aim is to solve the problem without taking explicit account of either emissivity or water vapor, but to account for their effects simultaneously. The difficulty in the first approach is that an estimation of the emissivity must be provided and validated; this requires global surface spectral emissivity information that is, unfortunately, currently unavailable [29].

In this work, we have chosen to develop an algorithm for the estimation of the air temperature close to the surface (canopy layer) following the second approach. We perform a multiple linear regression with pixel-by-pixel cloud free, calibrated day and night brightness temperatures T_{11} and T_{12} observed by the channels 11 and 12 of AATSR for the nadir view.

The linear regression formula implemented in order to retrieve the air temperature T_a very close to the surface from T_{11} and T_{12} is:

$$T_a = a_0 + a_1 T_{11} + a_2 (T_{11} - T_{12}) \tag{2}$$

where a_0, a_1, a_2 are the regression coefficients, depending simultaneously on atmospheric water vapor and land surface emissivity. Equation (2) was solved as an Ordinary Least Squares regression where the brightness temperatures and the air temperatures play the role of predictors and response variables respectively.

In order to study the tendency of UHIs, different coefficients for day and night, as well as for urban and rural areas, were computed exploiting the data set of Tables 1 and 2; these are summarized in Table 4. In particular, a data set of cloud-free brightness temperatures (T_{11} and T_{12}) and the corresponding T_a in time and space from the eight weather stations was selected from 2003 to 2005 for the computation of the regression coefficients (1,809 data samples). In order to match satellite-based and ground-based data, we utilized the AATSR pixels covering the weather station locations, selecting the air temperatures from the ground stations corresponding to the time closest to that of the satellite passes, with a maximum time difference of less than 30 minutes.

Table 4. Regression coefficients for the estimation of air temperature T_a in the Roma area (canopy layer) using AATSR brightness temperatures (channels 11 and 12). The satellite passes are around 9:00–10:00 and 20:00–21:00 UTC.

Regression Coefficients	Urban-Day	Urban-Night	Rural-Day	Rural-Night
a_0	177.33	16.17	184.7	76.83
a_1	0.35	0.95	0.34	0.72
a_2	2.62	1.10	2.53	2.32

Then, a validation test of the proposed approach was performed using the set of independent data of T_{11}, T_{12} and T_a belonging to 2006 (663 samples). For this independent test, the estimation of T_a using equation (2) showed accuracies in terms of rms error of about 3 K during the day, with better accuracies (about 2 K) during the night, when differential surface heating is absent.

6. Results and Discussion

UHI studies are generally conducted in one of two ways: measuring the UHI in air temperature through the use of automobile transects and weather station networks, and measuring the UHI in surface (or skin) temperature through the use of airborne or satellite remote sensing. *In situ* data have the advantage of a high temporal resolution and a long data record, but have poor spatial resolution. Conversely, remotely-sensed data have higher spatial distribution but low temporal resolution and a shorter data record.

In this paper, we have analyzed the UHI by both weather stations and satellite remote sensing, but with satellite maps targeted to the estimation of the air temperature in the canopy layer.

6.1. UHI Analysis from Weather Stations

A frequently used metric to describe the degree of development of the UHI is the heat island intensity, $\Delta T_{u\text{-}r}$. This is the difference in temperature between urban and rural locations within a given time period. The temperature measurements in the urban area were recorded by seven weather stations all situated in or near to the center of Rome, whereas the temperature measurements for the rural site were retrieved by a weather station named Pratica di Mare (Table 2).

In order to take advantage of the high temporal resolution of the *in situ* data, since each station records the air temperature every hour, the daily averaged trend of UHI intensity for each month was computed. The trend was obtained by subtracting the averaged monthly urban air temperature to the averaged monthly rural air temperature, for each year (2003–2006). Figure 3 reports this trend measured during 2003 by the Rome weather stations for the months corresponding to the higher UHI. Similar tendency was found for the other years.

This figure shows the CLHI intensity progressively increasing from midday and reaching a maximum (around 5 K) approximately a few hours later, remaining high through the night hours until predawn hours when levels begin to fall. During the day the CLHI is typically fairly weak or even negative (a cool island), probably due to areas that are shaded by tall buildings or other structures. The green line shows a negative CLHI intensity for the Villa Ada station, which is situated at the edge of a park. In fact, vegetation provides important shading effects as well as cooling through evaporation.

The CLHI analysis by ground station measurements points out how seasonal variations affect the heat island magnitude, with weak intensity in winter and reaching a maximum during summer when the amount of incoming solar radiation is greatest and artificial surfaces like asphalt tend to warm faster than those of the surrounding rural areas, acting as a reservoir of heat energy. Even the weather plays an important role, particularly wind and clouds. In fact, heat island magnitudes are largest under calm and clear weather conditions. Increasing winds mix the air and reduce the heat island and increasing clouds reduce radiative cooling at night, which in turn reduce the heat island [2].

Comparing the CLHI behavior with respect to the SHI, from literature we can infer that SHI is usually most distinct during the day when strong solar heating can lead to larger temperature differences between dry surfaces and wet, shaded, or vegetated surfaces [2,22].

Figure 2. Daily average trend of the UHI intensity $\Delta T_{u\text{-}r}$ measured by the seven meteorological stations across Rome over six months (in 2003). The red and blue circles are the positive and negative CLHI intensity, respectively. The green line is the Villa Ada trend.

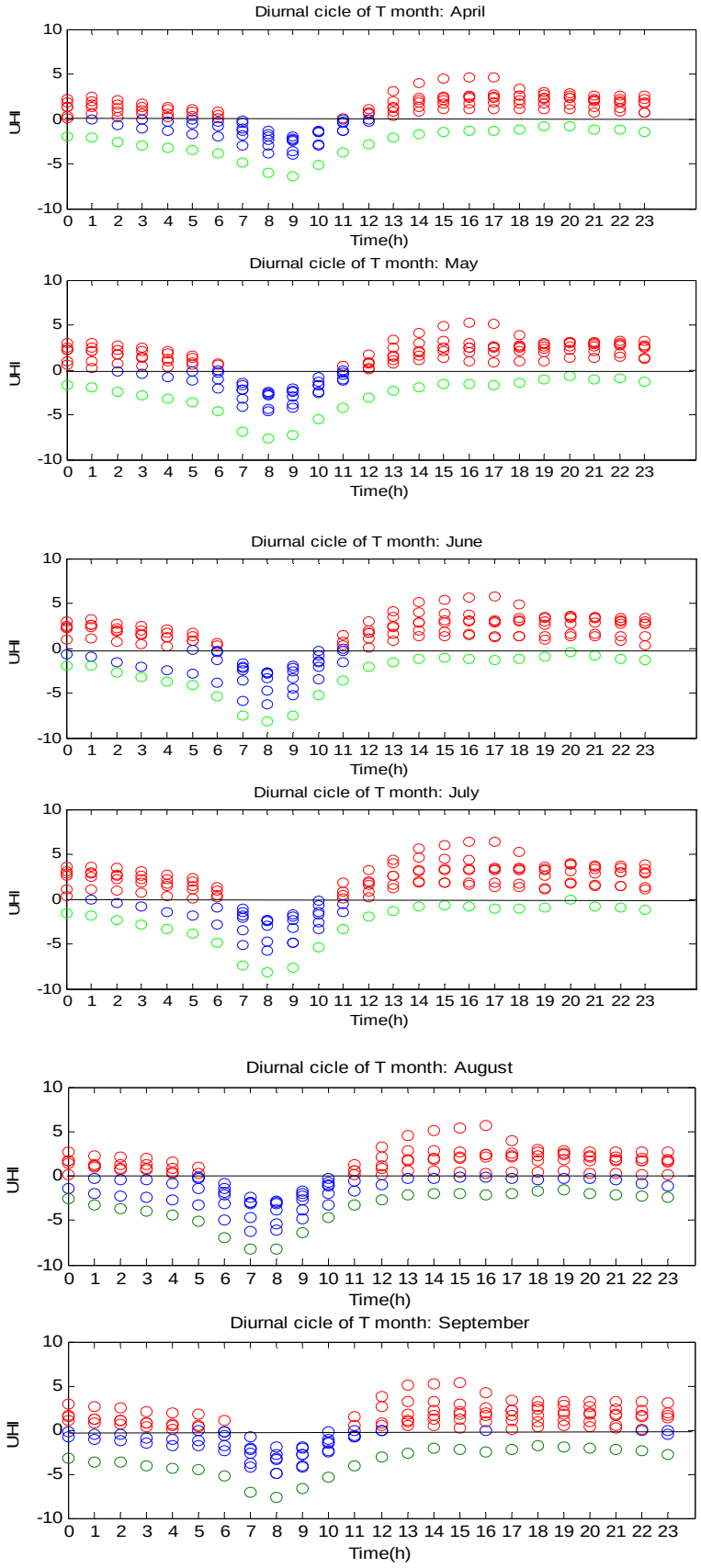

6.2. UHI Analysis from AATSR

The potential of analyzing the UHI with satellite-based sensors lies in the availability of maps with good spatial distribution and resolution (1 km or better).

Detailed maps of the air temperatures observed in the cities are currently not a routine part of the urban weather monitoring services provided by city authorities and by the meteorological offices. Furthermore, ground station networks are not homogeneously distributed and, in some locations, do not exist at all. Therefore, Earth Observation satellites, with their high spatial resolution, offer a means to characterize the UHIs and in general to provide more efficient urban meteorological services for the benefit of citizens.

An advantage of studying the UHI is that the quantity of interest is not the absolute urban temperature, but the difference in temperature between the urban and rural areas. Therefore some sources of systematic error in the temperature retrieval (radiometric calibration errors, variations in surface emissivity [21]) are thus partially removed in the differencing procedure [6].

In this section, the CLHI across Rome by means of the AATSR data was analyzed. In total, 634 daytime and nighttime scenes taken between 2003 and 2006 were processed, at around 9:00–10:00 and 20:00–21:00 UTC. Through the Equation (2), air temperature was retrieved in order to study the magnitude of the UHI pixel-by-pixel during day and night. Then, the intensity of CLHI, $\Delta T_{u\text{-}r}$, was obtained by subtracting the averaged monthly urban and rural air temperature in clear-sky conditions; both were estimated by applying the regression coefficients of Table 4. As an example, the results of $\Delta T_{u\text{-}r}$, during day and night in June, July and August 2003 are presented in Figure 4, where the main roads of Rome are reported in black (the city is chiefly located inside the motorway orbital road).

Figure 4. Monthly intensity of CLHI ($\Delta T_{u\text{-}r}$, [K]) in Rome, during summer 2003.

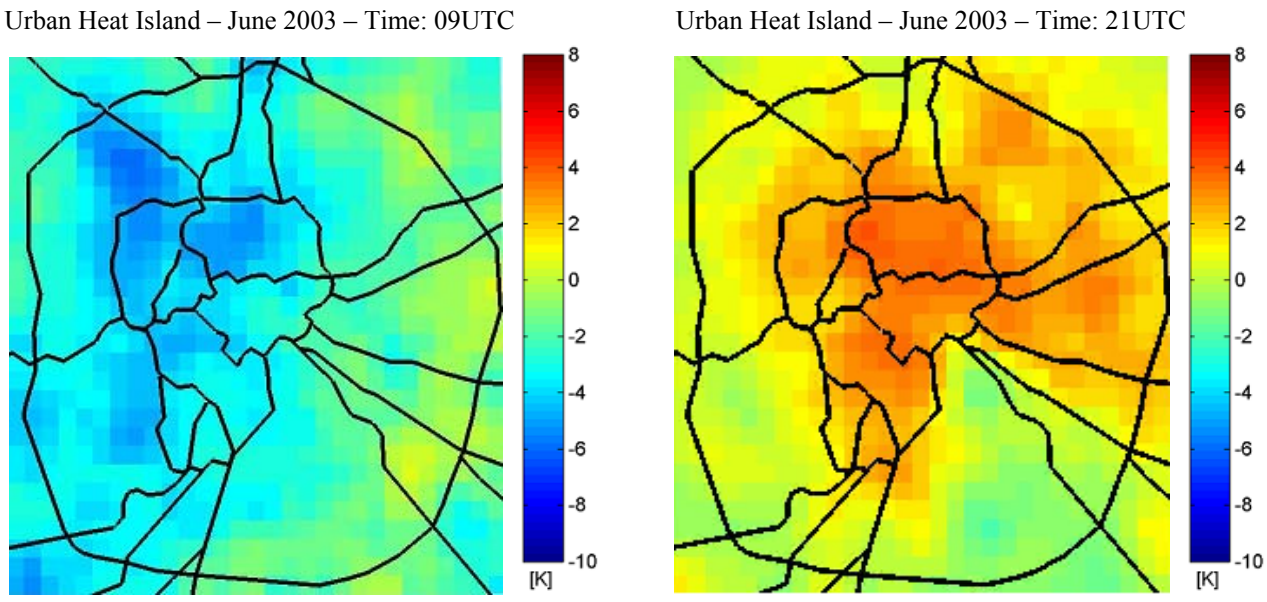

Figure 4. *Cont.*

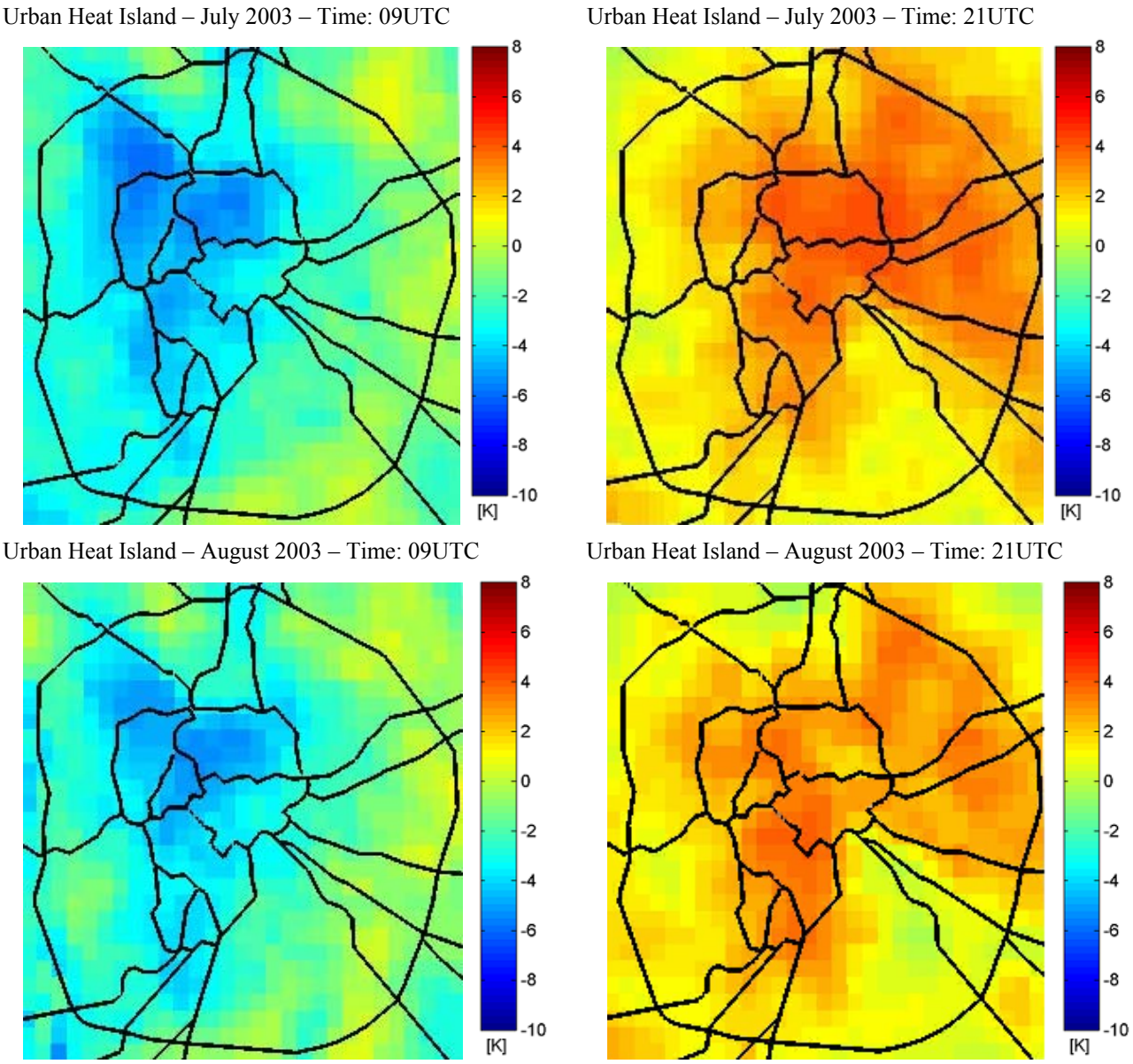

With reference to Figure 3, a $\Delta T_{u\text{-}r}$ of about 3–4 K is expected during the night (around 21:00 UTC) and a negative or almost zero CLHI intensity during the daytime (around 9:00 UTC). From Figure 4, the monthly maps of CLHI intensity from AATSR confirm this behavior. It should be noted that during the daytime the surface has not been warmed yet and the main contributions to heating are from anthropogenic sources like traffic which is more intense in the morning along the main roads, in particular along the South-East of the Rome ring road (Grande Raccordo Anulare). During the winter months, the contribution to heating of the main roads is detectable but much less intense, as expected. During the night, as expected, the UHI is particularly significant. Also, a greater nighttime $\Delta T_{u\text{-}r}$ during July 2003 was found, in addition to the fact that July 2003 was extremely hot.

Moreover, the nighttime maps reveal a greater $\Delta T_{u\text{-}r}$ in the center and East sides of Rome: this can be ascribed both to the presence of the more densely built up areas of the city, as sketched in Figure 2, and to the presence of a typical evening breeze from the sea in the West side (named “Ponentino”),

playing an important role in the western mitigation of the CLHI intensity, since heat island magnitudes are largest under calm weather conditions.

The UHI behavior noticed in the monthly maps is also confirmed analyzing a map for a specific day: as an example, the $\Delta T_{u\text{-}r}$ for the 20th August 2003 is shown in Figure 5, where an intense heat island was detected.

Figure 5. Intensity of CLHI ($\Delta T_{u\text{-}r}$, [K]) in Rome on the 20th August 2003.

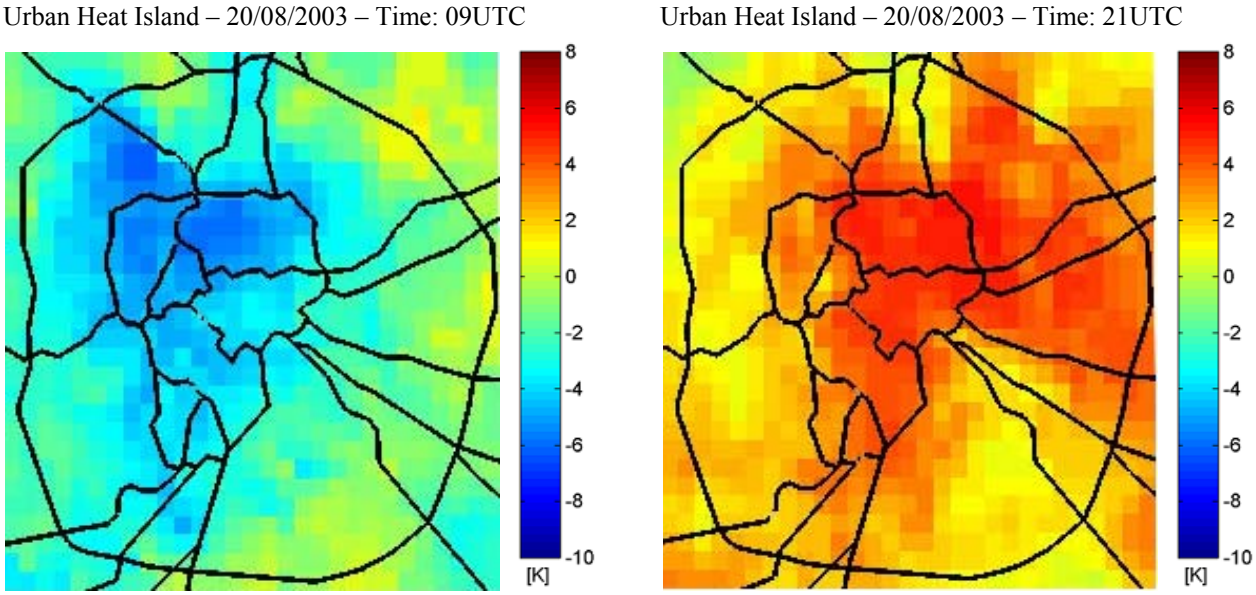

Therefore, the processing of satellite data for UHI intensity detection is able to monitor not only the additional heating effects of the main roads with intense traffic, seasonal dependent, and of the particularly densely built-up areas, but also is able to detect slight cooling effects due to particular weather phenomena. With cities becoming more densely populated and with a growing recourse to artificial surfaces, this remote sensing application proves extremely useful (e.g., health issues).

7. Conclusions

In this work, the UHI of Rome was analyzed using both ground-based weather stations and the satellite-based AATSR sensor. First, UHI spatial characteristics were assessed using air temperatures measured by the weather stations, then UHI maps were produced using brightness temperatures from AATSR. Satellite derived maps confirmed, during summer months, an average intensity of CLHI of about 3–4 K during nighttime and a negative or almost zero CLHI intensity during daytime. The UHI intensity reaches a maximum during summer when the amount of incoming solar radiation is greatest, because artificial surfaces like asphalt tend to warm more intensively than those of surrounding rural areas, acting as a reservoir of heat energy.

During the morning, the urban surface warming is mainly due to traffic, which is more intense along the main roads, while during the night the UHI is evident especially in the center and East sides of Rome, which are also the more densely built up areas of the city.

Acknowledgements

The authors wish to thank the European Space Agency (ESA/ESRIN) for the availability of the satellite data, and ARPA Lazio for the ground data. The authors thank Marc Paganini and Stefano Casadio of the ESA/ESRIN for the support during this work.

References

1. Oke, T.R. *Boundary Layer Climates*, 2nd ed.; Routledge: London, UK, 1987; p. 435.
2. Voogt, J.A. *Urban Heat Island: Hotter Cities*. ActionBioscience: North Port, FL, USA, 2004. Available online: http://www.actionbioscience.org/environment/voogt.html (accessed on 19 May 2010).
3. Oke, T.R. City size and the urban heat island. *Atmos. Environ.* **1973**, *7*, 769-779.
4. Voogt, J.A.; Oke, T.R. Thermal remote sensing of urban climates. *Remote Sens. Environ.* **2003**, *86*, 370-384.
5. Rao, P.K. Remote sensing of "Urban Heat Islands" from an environment satellite. *Bull. Am. Meteorol. Soc.* **1972**, *53*, 647-448.
6. Streutker, D.R. Satellite-measured growth of the urban heat island of Houston, Texas. *Remote Sens. Environ.* **2003**, *85*, 282-289.
7. Lee, H.Y. An application of NOAA AVHRR thermal data to the study of urban heat islands. *Atmos. Environ.* **1993**, *27B*, 1-13.
8. Dousset, B.; Gourmelon, F. Surface temperatures of the Paris basin during summertime, using satellite remote sensing data. In *Proceedings of the 5th International Conference on Urban Climate*, Lodz, Poland, September 2003.
9. Hung, T.; Uchihama, D.; Ochi, S.; Yasuoka, Y. Assessment with satellite data of the urban heat island effect in Asian mega cities. *Int. J. Appl. Earth Obs. Geoinf.* **2006**, *8*, 34-48.
10. Colacino, M.; Lavagnini, A. Evidence of the urban heat island in Rome by climatological analyses. *Theor. Appl. Climatol.* **1982**, *31*, 87-97.
11. Huot, J.P.; Tait, H.; Rast, M.; Delwart, S.; Bézy, J.L.; Levrini, G. The optical imaging instruments and their applications: AATSR and MERIS. *ESA Bull.* **2001**, *106*, 56-66.
12. Llewellyn-Jones, D.; Edwards, M.; Mutlow, C.; Birks, A.; Barton, I.; Tait, H. AATSR: Global-change and surface-temperature measurements from Envisat. *ESA Bull.* **2001**, *105*, 11-21.
13. European Space Agency. *Envisat AATSR Product Handbook*; Issue 2.2, ESA: Paris, France, 2007. Available online: http://envisat.esa.int/pub/ESA_DOC/ENVISAT/AATSR/aatsr.ProductHandbook.2_2.pdf (accessed on 19 May 2010).
14. Fischer, J. MERIS for atmospheric applications. In *Proceedings of the MERIS/AATSR Workshop*, ESA-Esrin, Frascati, Italy, October 2005.
15. European Space Agency. *Envisat MERIS Product Handbook*; Issue 2.1, ESA: Paris, France, 2006. Available online: http://envisat.esa.int/pub/ESA_DOC/ENVISAT/MERIS/meris.ProductHandbook.2_1.pdf (accessed on 19 May 2010).
16. Grey, W.M.F.; North, P.R.J.; Los, S.O.; Mitchell, R.M. Aerosol optical depth and land surface reflectance from multiangle AATSR measurements: Global validations and intersensor comparisons. *IEEE Trans. Geosci. Remote Sens.* **2006**, *44*, 2184-2197.

17. Smith, D.L. Intercalibration of AATSR and MERIS reflectances. In *Proceedings of the MERIS/AATSR Workshop*, ESA-Esrin, Frascati, Italy, September 2003.
18. McMillin, L.M. Estimation of sea surface temperature from two infrared window measurements with different absorption. *J. Geophys. Res.* **1975**, *80*, 511-5117.
19. Li, Z.L.; Becker, F. Feasibility of land surface temperature and emissivity determination from AVHRR data. *Remote Sens. Environ.* **1993**, *43*, 67-85.
20. Price, J.C. Assessment of the urban heat island effect through the use of satellite data. *Mon. Weather Rev.* **1979**, *107*, 1554-1557.
21. Price, J.C. Land surface temperature measurements from the split window channels of the NOAA 7 AVHRR. *J. Geophys. Res.* **1984**, *D5*, 7231-7237.
22. Roth, M.; Oke, T.R.; Emery, W.J. Satellite-derived urban heat island from three coastal cities and the utilization of such data in urban climatology. *Int. J. Remote Sens.* **1989**, *10*, 1699-1720.
23. Ulivieri, C.; Castronuovo, M.M.; Francioni, R.; Cardillo, A. A split-window algorithm for estimating land surface temperature from satellites. In *Proceedings of COSPAR*, Washington, DC, USA, September 1992.
24. Vázquez, D.P.; Olmo Reyes, F.J.; Arboledas, A.L. A comparative study of algorithms for estimating land surface temperature from AVHRR data. *Remote Sens. Environ.* **1997**, *62*, 215-222.
25. Prata, A.J.; Platt, C.M.K. Land surface temperature measurements from the AVHRR. In *Proceedings of the 5th AVHRR Data Users Meeting*, Tromso, Norway, June 1991; pp. 433-438.
26. Voogt, J.A.; Oke, T.R. Effects of urban surface geometry on remotely-sensed surface temperature. *Int. J. Remote Sens.* **1998**, *19*, 895-920.
27. Oke, T.R. *Boundary Layer Climate*, 2nd ed.; Routledge: London, UK, 1987.
28. Taylor, S.E. Measured emissivity of soils in the south-east United States. *Remote Sens. Environ.* **1979**, *8*, 359-364.
29. Prata, A.J. *Land Surface Temperature Measurement from Space: AATSR Algorithm Theoretical Basis Document*; Contract Report to ESA, CSIRO Atmospheric Research: Aspendale, Australia, 2002.